Polymer Journal (2015) 47, 195–200

www.nature.com/pj

ORIGINAL ARTICLE

Luminescence of fusion materials of polymeric chain-structured lanthanide complexes

Saki Sato[1], Ayumi Ishii[1], Chisaki Yamada[1], Junguen Kim[2], Chul Ho Song[2,4,5], Akihiko Fujiwara[2], Masaki Takata[3] and Miki Hasegawa[1]

Polymeric chain-structured complexes were prepared with helical lanthanide complexes (LnL; Ln = Eu^{III}, Tb^{III}, Gd^{III}) and benzene-dicarboxylate derivatives (benzene-1,4-dicarboxylate (bdc), 2-aminoterephtalate (atpa) and 2-hydoloxyterephtalate (htpa)), which show some noteworthy physicochemical properties, photoluminescence and thermal stabilities. The complex EuL-bdc shows bright luminescence originating from Eu^{III} by UV excitation. The emission color can be tuned by mixing with TbL. The structures of these chain complexes were clarified with synchrotron X-ray powder diffraction measurements. The derivation of the linker moiety (bdc, atpa or htpa) was found to affect the intermetal energy transfer from Tb^{III} to Eu^{III}.
Polymer Journal (2015) **47,** 195–200; doi:10.1038/pj.2014.88; published online 5 November 2014

INTRODUCTION

Fusion materials of metal and organic ligands have great potential for use as multifunctional materials with luminescence, magnetism, catalytic activity, gas storage and separation. For instance, porous coordination polymers (PCPs), metal-organic frameworks (MOFs) or other molecular networks have attracted much attention because of their tunable structures, thermal stabilities and potential applications as functional materials.[1–6]

Recently, PCPs or MOFs based on lanthanide ions (Ln) have been reported as highly luminescent materials.[7–14] Emissions from these materials are originated from ff transitions of the Ln ion that occur at inner unoccupied 4*f* orbitals shielded by the occupied 5*s* and 5*p* orbitals. Europium (Eu^{III}) and terbium (Tb^{III}) complex with organic ligands as photo antennas and exhibit red- and green-colored emission, respectively, by UV excitation.[15,16] García and co-workers[17] reported two series of isoreticular chiral MOFs assembled from Ln(III), Na(I) and chiral flexible-achiral rigid dicarboxylate ligands in which Ln(III) forms a polyhedron structure with oxygen ions of the dicarbozylate ligand. These materials show tunable UV–vis–IR light emission through an effective Ln(III) sensitized via dicarbozylate ligands at room temperature. Deacon and co-workers[18] demonstrated one-dimensional coordination polymers of lanthanide trichloride hydrates and dibenzoylmethane with Cs or K ions. In these systems, unfortunately, undesirable energy back transfer occurs that reduces luminescence quantum yields. The thermostability of PCPs and MOFs has been widely investigated.[19–24] Chen and co-workers[19] first reported temperature-sensitive three-dimensional MOFs with heterolanthanide ions linked by 2,5-dimethoxy-1,4-benzendicarboxylate. These mixed lanthanide MOFs have enabled energy transfer among the Ln ions and temperature-sensitive luminescence of the Ln ions. Hasegawa and co-workers[20] also investigated a thermosensing coordination polymer of an Eu(III) and Tb(III) complex with hexafluoro acetylacetonato as the ligand and 4,4′-bis (diphenylphosphoryl)biphenyl as the linker. This coordination polymer exhibits a high emission quantum yield and temperature sensitivity with a stability range of 200–500 K.

These PCPs and MOFs with a one- or three-dimensional structure can be obtained as a single crystal with high symmetry around the Ln ion.[25] The formation of these structures, however, involves a multistep process spanning from the synthesis of molecular materials to crystallization. In addition, higher symmetry around the Ln ion in PCPs and MOFs tends to lower the emission intensity. To obtain highly luminescent Ln compounds in a simple process, we propose the construction of a novel chain structure with helical lanthanide complexes (Ln**L**; Ln = Eu^{III}, Tb^{III}, Gd^{III}) and dicarboxylate derivatives. Ln**L** has a single helical structure with a hexadentate ligand of two bipyridine moieties bridged by an ethylenediamine unit, which shows strong ff emissions through an effective energy transfer from a helical ligand to a metal ion.[26] Eu**L** shows bright emission with a quantum yield greater than 50% both at 77 K and at room temperature in the solid state. In contrast, the luminescence quantum yield for Tb**L** is significantly dependent on the temperature. Here, two nitrate ions of EuL or TbL are replaced by benzene-dicarboxylate derivatives (benzene-1,4-dicarboxylate (bdc), 2-aminoterephtalate (atpa) and

[1]College of Science and Engineering, Aoyama Gakuin University, Kanagawa, Japan; [2]JASRI/SPring-8, Hyogo, Japan and [3]RIKEN/SPring-8, Hyogo, Japan
[4]Current address: GREEN, National Institute for Materials Science, 1-1 Namiki, Tsukuba, Ibaraki 305-0044, Japan.
[5]Current address: NIMS Beamline Station at SPring-8, National Institute for Materials Science, 1-1-1 Kouto, Sayo-cho, Sayo-gun, Hyogo 619-5198, Japan.
Correspondence: Professor Dr M Hasegawa, College of Science and Engineering, Aoyama Gakuin University, 5-10-1 Fuchinobe, Chuo-ku, Sagamihara, Kanagawa 252-5258, Japan.
E-mail: hasemiki@chem.aoyama.ac.jp
Received 31 July 2014; revised 22 August 2014; accepted 31 August 2014; published online 5 November 2014

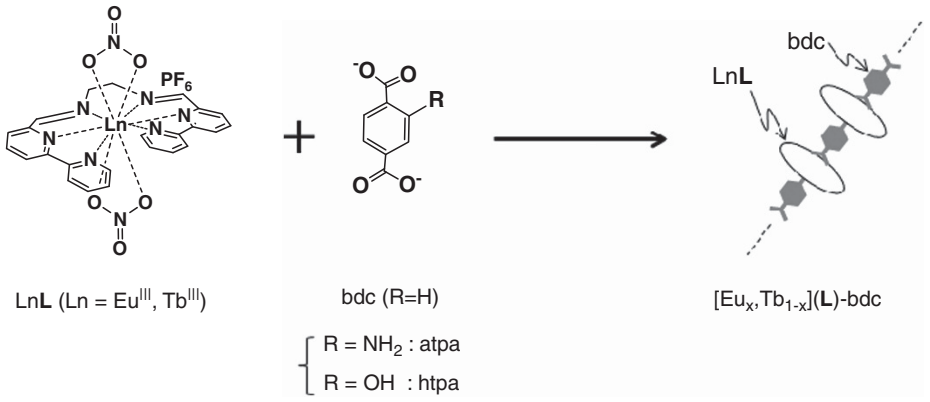

Figure 1 The molecular structures of Ln**L** and benzene-dicarboxylate derivatives (bdc: benzene-1,4-dicarboxylate, atpa: 2-aminoterephtalate, htpa: 2-hydoloxyterephtalate).

2-hydoloxyterephtalate (htpa)), resulting in a chain coordination compound that maintained its helical molecular structure and the electronic state of the complex. Our chain structure of the Ln complexes with high regularity can be simply constructed by mixing Ln**L**s and a linker, not by crystallization. Such a facile construction process of the fusion materials is very useful for their application as functional materials.

In this paper, we report on the fabrication of novel chain-structured mixed lanthanide complexes: $[Eu_x,Tb_{1-x}]$(**L**)-bdc, $[Eu_x,Tb_{1-x}]$(**L**)-atpa and $[Eu_x,Tb_{1-x}]$(**L**)-htpa. Polymerized structures of these chain complexes were clarified by synchrotron X-ray powder diffraction (XRPD) observations. Moreover, the thermal stability and luminescence properties were characterized by the absolute emission quantum yield, from emission lifetime measurements, and using thermogravimetric analysis. Depending on the linker and chain network structure, the chain-structured lanthanide complexes show dual emissions from each metal ion and/or sensitized emissions through the metal-to-metal energy transfer (MMEnT).

MATERIALS AND METHODS

Materials and synthesis

Most reagents and solvents were used without further purification. Eu**L** ([Eu(**L**)$(NO_3)_2$](PF_6)), Tb**L** ([Tb(**L**)$(NO_3)_2$](PF_6)) and Gd**L** ([Gd(**L**)$(NO_3)_2$](PF_6)) were synthesized as previously reported.[26] $[Eu_x,Tb_{1-x}]$(**L**)-bdc was obtained by the reaction of Eu**L** (x mmol, $0 \leqslant x \leqslant 1$) and Tb**L** (1-x mmol) with Na_2bdc (0.1 mmol) in acetonitrile for 24 h. The resulting solid was obtained as a microcrystalline white powder (60–80% yield). $[Eu_x,Tb_{1-x}]$(**L**)-atpa and $[Eu_x,Tb_{1-x}]$(**L**)-htpa were also prepared with H_2atpa and H_2htpa, respectively. An ethanol solution of H_2atpa or H_2htpa with 1 equiv of triethylamine was added to an acetonitrile solution of Ln**L** and stirred for 48 h, resulting in a white yellow precipitate (50–60% yield).

Measurements

The Fourier-transform infrared spectroscopy (FT-IR) spectra were recorded on a FT-720 spectrometer (Horiba Ltd., Kyoto, Japan). X-ray photoelectron spectroscopy (XPS) measurements were recorded on a KRATOS AXIS ULTRA DLD (Shimadzu Corporation, Kyoto, Japan) equipped with a monochromatic Al-Kα X-ray source (1253.6 eV); the binding energies were calibrated at the Au 4*f* level (84.0 eV). Synchrotron XRPD experiments were performed on a large Debye-Scherrer camera installed at SPring-8 BL02B2 (SPring-8/JASRI, Hyogo, Japan), using an imaging plate as the detector.[27,28] Nitrogen (N_2) gas flow systems were installed for low-temperature experiments (300 ~ 77 K). The wavelength of the incident X-ray was 0.9997 Å for Ln**L**-bdc and 1.0009 (1) Å for the other two series (Ln**L**-atpa and Ln**L**-htpa). TGA and differential thermal analysis were performed using a DTG-50 instrument (Shimadzu Corporation) under a nitrogen atmosphere and at a heating rate of 10 °C min^{-1}.

Electronic absorption and luminescence spectra were recorded on a UV-3100 (Shimadzu Corporation) with an absolute specular reflectance attachment and a Jobin-Ybon Fluorolog 3–22 (Horiba Ltd.), respectively. The emission decay curves were measured using a Quantaurus-Tau C11367-12 (Hamamatsu Photonics K. K., Hamamatsu, Japan) excited by a Xenon flash lamp with a band-path filter ($\lambda_{ex} = 340$ nm). The fluorescence quantum yields were measured using the C9920-02 Absolute PL Quantum Yield Measurement System (Hamamatsu Photonics K. K.).[29–31]

RESULTS AND DISCUSSION

Structure characterization

$[Eu_x,Tb_{1-x}]$(**L**)-bdc was synthesized by mixing Eu**L** ($0 \leqslant x \leqslant 1$) and Tb**L** ($1-x$) with Na_2bdc in acetonitrile for 24 h (Figure 1). The two nitrate ions of Ln**L**, binding to the Ln from both apical sites, were exchanged by the carboxyl group of bdc, forming the chain structure of $[Eu_x,Tb_{1-x}]$(**L**)-bdc. The coordination bond between bdc and Ln**L** was confirmed from the FT-IR spectra, in which the disappearance of the two N-O stretching vibrations of the nitrate ion at 1470 cm^{-1} (asymmetric) and 1286 cm^{-1} (symmetric) was observed (Supplementary Figure S1). The replacement of the nitrate ion was also confirmed by XPS measurements (Supplementary Figure S2). Ln**L** shows the N 1s XPS bands at 396.5 and 404.0 eV originating from the ligand L and the nitrate ion in the complex, respectively. The N 1s XPS band of the nitrate ion in Ln**L** disappeared to form the chain complex. The mixing ratio of Eu/Tb in the chain complex corresponded to the concentration ratios of Eu**L** and Tb**L**, the source materials of the chain compound, as determined by XPS analysis (Supplementary Table S1).

The structures of these chain complexes were clarified in the XRPD measurements. Figure 2 shows the XPRD patterns of Eu**L**-bdc, Tb**L**-bdc and $[Eu_{0.5},Tb_{0.5}]$(**L**)-bdc. For comparison, the XRPD of a 1:1 mechanical mixture of Eu**L**-bdc and Tb**L**-bdc was also measured and is shown in Figure 2. Each diffraction pattern is observed with sharp peaks, indicating a high regularity of the structure. Tb**L**-bdc shows diffraction peaks mainly at 4.01, 5.58, 5.97, 6.85, 7.96, 11.1 and 13.8°, which are assigned to the Bragg reflections of (010), (100), (10-1), (1-10), (020), (200) and (220), respectively. The chain structure of Tb**L**-bdc belongs to the monoclinic system ($P\bar{1}$: $Z = 2$) with unit cell parameters of $a = 12.29$ Å, $b = 14.36$ Å, $c = 10.12$ Å, $\alpha = 90.0°$, $\beta = 123.35°$ and $\gamma = 90.0°$. The length of the b axis (14.36 Å) corresponds to the estimated interchain distance of Tb**L**-bdc, where Tb**L** has a molecular width of 12.6 Å (Figure 3a). In the chain structure, the Ln ion exists at intervals of 12.29 Å along with the a axis in which the Ln ions are linked by the bdc molecules (Figure 3b).[26,32] After mixing Eu**L** in the Tb**L**-bdc chain structure, the

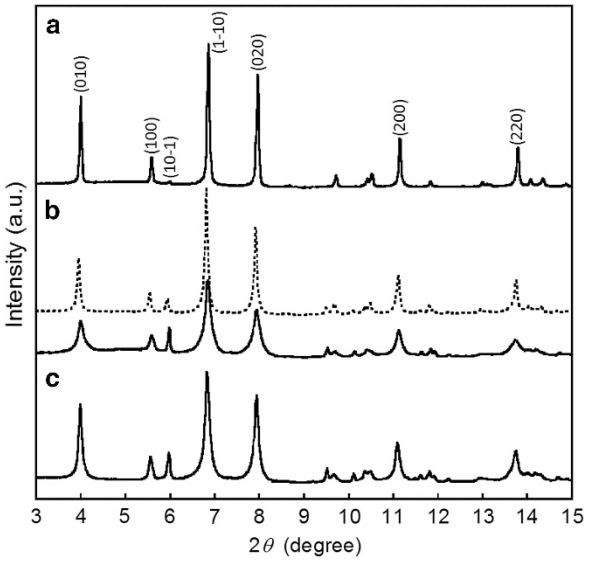

Figure 2 The synchrotron X-ray powder diffraction patterns of (**a**) Tb**L**-bdc, (**b**) [$Eu_{0.5}$,$Tb_{0.5}$](**L**)-bdc and (**c**) Eu**L**-bdc, together with the Bragg reflection assignments. The dotted line (**b**) shows the XRPD of a 1:1 mechanical mixture of Eu**L**-bdc and Tb**L**-bdc.

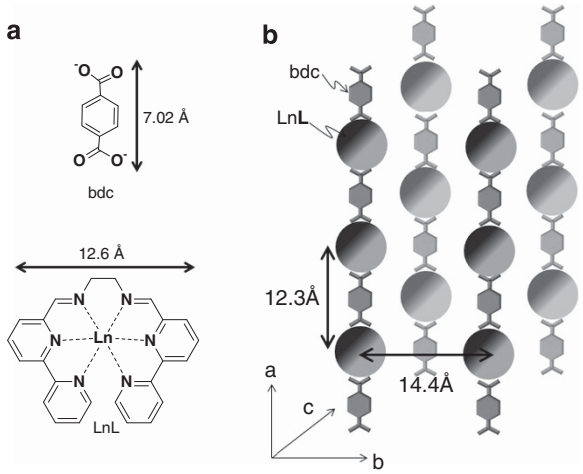

Figure 3 (**a**) The molecular structure and molecule size estimated from single crystal X-ray analysis.[26,32] (**b**) The schematic structure of [$Eu_{0.5}$,$Tb_{0.5}$](**L**)-bdc along with the *ab* plane.

diffraction peaks were broadly observed at almost the same positions as those of Tb**L**-bdc. The broader diffractions indicate the partial formation of an amorphous-like structure. Notably, the (10-1) diffraction peak at 5.58° strongly appears in [$Eu_{0.5}$,$Tb_{0.5}$](**L**)-bdc. This peak suggests that there is another chain at a 0.5 unit difference along each axis, that is, the chain arrangement of [$Eu_{0.5}$,$Tb_{0.5}$](**L**)-bdc is different from that of Tb**L**-bdc. The XRD pattern of [$Eu_{0.5}$,$Tb_{0.5}$](**L**)-bdc does not correspond with that of the 1:1 mechanical mixture of Eu**L**-bdc and Tb**L**-bdc. These results support the observation that Eu**L** and Tb**L** are uniformly ordered in the crystal to create a new chain arrangement.

[Eu_x,Tb_{1-x}](**L**)-atpa and [Eu_x,Tb_{1-x}](**L**)-htpa were also obtained by the same synthesis procedure as [Eu_x,Tb_{1-x}](**L**)-bdc. The substituent group of atpa and htpa (-NH_2 and -OH, respectively) allows a chain to interact with another one. Observations using FT-IR and XPS confirmed that atpa and htpa acted as linkers between the Ln**L**s and other chains (Supplementary Figures S3 and Supplementary Tables S2). The XPRD spectra of [Eu_x,Tb_{1-x}](**L**)-atpa and [Eu_x,Tb_{1-x}](**L**)-htpa are shown in Supplementary Figure S5. These complexes only exhibit a halo pattern of the glass substrate, that is, Eu**L** and Tb**L** form an amorphous structure by connecting with atpa or htpa as a linker. In [Eu_x,Tb_{1-x}](**L**)-atpa and [Eu_x,Tb_{1-x}](**L**)-htpa, the substituent group of atpa and htpa (-NH_2 and -OH, respectively) can interact with the metal ion of the complex or another linker through coordination or a hydrogen bond, resulting in the formation of a new network structure with a chain-structured complex.

To evaluate the thermal stability of the chain-structured lanthanide complexes, TGA and differential thermal analysis of Eu**L**-bdc, Eu**L**-atpa, Eu**L**-htpa and Eu**L** were measured under a nitrogen atmosphere at a heating rate of 10 °C min^{-1} (Supplementary Figure S6). The coordination bonding of bdc to Ln was strong; therefore, the chain structure of Ln**L** constructed by bdc was maintained until the temperature increased to 280 °C. Eu**L**-bdc shows an exotherm at 247.6 °C, assigned to the decomposition of the ligand **L** in Ln**L**, and an endotherm at 150 °C because of the release of some components such as NO_3^- or solvents. In contrast, Eu**L**-atpa and Eu(**L**)-htpa have a decomposition point at 387.1 °C and 388.0 °C, respectively. The high thermal stabilities of [Eu_x,Tb_{1-x}](**L**)-atpa and [Eu_x,Tb_{1-x}](**L**)-htpa may be because of their amorphous network structure. In addition, the photophysical properties of the chain-structured complex were retained after a heating treatment at ~200 °C (Supplementary Figure S7).

Luminescence properties

Lanthanide complexes exhibit a high color purity emission from the metal ion induced by the photoexcitation of the organic ligands through an intramolecular energy transfer. To explain the energy transfer pathway in the lanthanide complex, the energy donor level of the ligand needs to be estimated because the energy accepter level of the trivalent lanthanide ion seldom changes in any environment.

The chain complexes Ln**L**-bdc show $\pi\pi^*$ absorption bands at 250 and 315 nm in the solid state (Supplementary Figure S8). The former band originates from the bdc and the latter from the ligand of Ln**L**. Ln**L**-atpa and Ln**L**-htpa also show absorption bands corresponding to the $\pi\pi^*$ transitions of the Ln**L** and linkers.

To estimate the energy donor level of Ln**L**-bdc, the luminescence spectrum of Gd**L**-bdc was examined. Gd^{III} has no appropriate accepter level for energy transfer from the organic ligands and only shows the ligand emissions. Thus, the Gd^{III} complexes provide important information regarding the energy transfer pathway. Gd**L**-bdc exhibits a broadened emission band at ~520 nm corresponding to the phosphorescence band of Gd**L** observed at ~500 nm (Supplementary Figure S9). The bdc bonding to Gd^{III} does not luminesce near this location. Specifically, a triplet level of **L** works as the energy donor level in Ln**L**-bdc. The red-shift of the phosphorescence bands in the chain structure seems to indicate that the substituent group or π electron of the linker interacts with the π electron system of **L**. Gd**L**-atpa and Gd**L**-htpa also show phosphorescence bands originating from **L** at 530 and 514 nm, respectively, and the phosphorescence level acts as the energy donor to the lanthanide *f* levels.

The luminescence and the excitation spectra of [Eu_x,Tb_{1-x}](**L**)-bdc in the solid state are shown in Figure 4 and Supplementary Figure S10, respectively. At room temperature, Tb**L**-bdc shows very weak ff emissions at 489, 544, 585 and 622 nm, which are assigned to the $^5D_4 \rightarrow {}^7F_6$, $^5D_4 \rightarrow {}^7F_5$, $^5D_4 \rightarrow {}^7F_4$ and $^5D_4 \rightarrow {}^7F_3$ transitions, respectively. Strong corresponding emission bands were observed at 77 K.

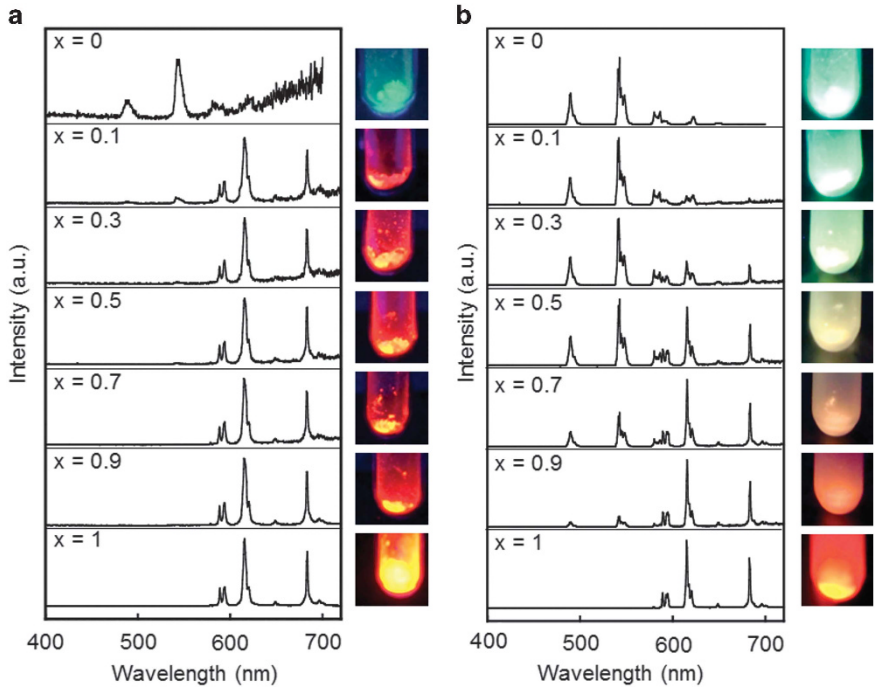

Figure 4 The luminescence spectra of $[Eu_x,Tb_{1-x}]$(**L**)-bdc in the solid state (**a**) at room temperature and (**b**) at 77 K ($\lambda_{ex}=315$ nm), together with photographs of each solid sample.

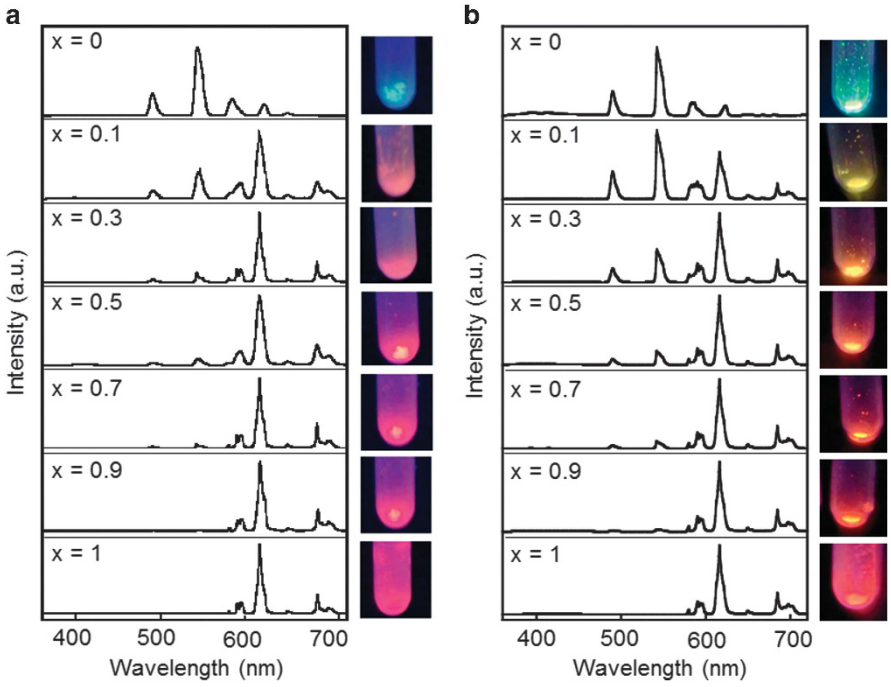

Figure 5 The luminescence spectra of (**a**) $[Eu_x,Tb_{1-x}]$(**L**)-atpa and (**b**) $[Eu_x,Tb_{1-x}]$(**L**)-htpa in the solid state at 77 K ($\lambda_{ex}=315$ nm), together with photographs of each solid sample.

The absolute luminescence quantum yield ϕ_{ff} and the luminescence lifetime τ_{ff} of Tb^{III} at room temperature were ~1% and 0.10 ms, respectively, which remarkably increased to 44.9% and 1.0 ms at 77 K. Meanwhile, Eu**L**-bdc exhibited strong emissions of Eu^{III} at 579, 592, 616, 649 and 683 nm, which are assigned to the $^5D_0 \rightarrow {}^7F_0$, $^5D_0 \rightarrow {}^7F_1$, $^5D_0 \rightarrow {}^7F_2$, $^5D_0 \rightarrow {}^7F_3$ and $^5D_4 \rightarrow {}^7F_4$ transitions, respectively. At room temperature, these emissions are observed with a ϕ_{ff} of 17.6% and a τ_{ff} of 1.5 ms, which are not significantly different from the results at 77 K (23.4% and 1.6 ms). These results indicate that the temperature sensitivity of Tb^{III} is much larger than that of Eu^{III} in the Ln**L**-bdc chain structure, which is caused by an effective back energy transfer from the emitting level of Tb^{III} to the triplet state of **L** in Tb**L**-bdc.[26]

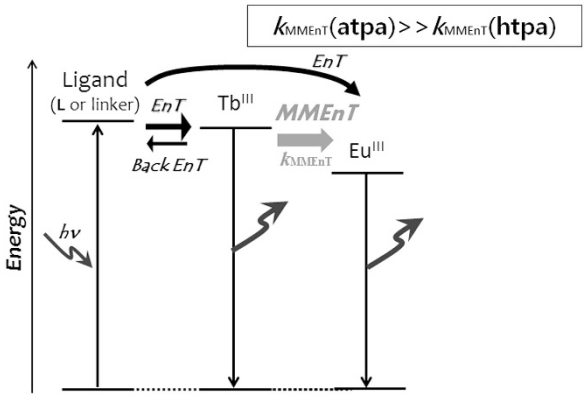

Figure 6 The schematic energy diagram of $[Eu_x,Tb_{1-x}]$(**L**)-atpa and $[Eu_x,Tb_{1-x}]$(**L**)-htpa. *EnT* and k_{MMEnT} refer to the rate constant of energy transfer and the metal-to-metal energy transfer, respectively.

At room temperature, the very weak Tb^{III} emission in $[Eu_x,Tb_{1-x}]$(**L**)-bdc was because of the large quenching process with the thermal equilibrium between the emitting level of Tb^{III} and the triplet state of **L**.

$[Eu_x,Tb_{1-x}]$(**L**)-bdc exhibited both emissions from Eu**L** and Tb**L,** and the emission color gradually changed depending on the mixing ratio of Eu^{III} and Tb^{III}. At room temperature, strong emissions of Eu^{III} appeared with a little mixing of Eu**L** in the Tb**L**-bdc. However, the emission behavior at room temperature is difficult to discuss because of the large thermal equilibrium of Tb^{III}, as already described.

Notably, a white emission color was successfully obtained from $[Eu_{0.5},Tb_{0.5}]$(**L**)-bdc at 77 K with chain structure formation of the red emissive Eu**L**, the green emissive Tb**L** and a linker, which was achieved only by a mixing process. The luminescence lifetimes of Eu^{III} and Tb^{III} in $[Eu_x,Tb_{1-x}]$(**L**)-bdc were not noticeably changed by the mixing ratio and were almost the same as those of Eu**L**-bdc and Tb**L**-bdc (Supplementary Table S4). Thus, these results indicate that the electronic structure of Eu**L** and Tb**L** is independently maintained without intermolecular or intermetal interactions among neighboring molecules, even in $[Eu_x,Tb_{1-x}]$(**L**)-bdc (Supplementary Figure S11).

To discuss the effect of the network structures with a characteristic substituent group on the emission of Ln**L**, we obtained the emission spectra of other chain complexes with atpa and htpa as a linker. $[Eu_x,Tb_{1-x}]$(**L**)-atpa and $[Eu_x,Tb_{1-x}]$(**L**)-htpa also show emissions from Eu**L** and Tb**L** at corresponding positions with $[Eu_x,Tb_{1-x}]$(**L**)-bdc at 77 K (Figure 5). However, the changes in emission intensity and color with the mixing ratio of these two chain-structured complexes differ from that of the $[Eu_x,Tb_{1-x}]$(**L**)-bdc. Thus, it suggests that another energy relaxation process occurs in $[Eu_x,Tb_{1-x}]$(**L**)-atpa and $[Eu_x,Tb_{1-x}]$(**L**)-htpa.

The emission decay curve of Eu**L** in Eu**L**-atpa can be divided into two components at 0.21 and 0.60 ms in the luminescence lifetimes at 77 K, meaning that two Eu^{III} sites exist with different symmetries in Eu**L**-atpa. Eu**L**-htpa also has two luminescent Eu components at 0.81 and 0.30 ms from the emission decay curves at 77 K. Because the XRPD pattern of $[Eu_x,Tb_{1-x}]$(**L**)-atpa or $[Eu_x,Tb_{1-x}]$(**L**)-htpa is broadened as described above, it is suitable to assume that the Ln**L** will bind/interact not only with the carboxylate group to build the main chain structure but also with the substituent amine or hydroxyl group, resulting in amorphous networks.

To evaluate the MMEnT from Tb^{III} to Eu^{III}, the luminescence lifetime of Tb was investigated. The emission intensity and lifetimes of Tb**L** in $[Eu_x,Tb_{1-x}]$(**L**)-atpa clearly decrease with an increase in the concentration ratios of Eu^{III} at 77 K. Tb^{III} in $[Eu_x,Tb_{1-x}]$(**L**)-atpa shows a characteristic emission decay curve (Supplementary Figure S12), meaning that the excitation energy transfer from Tb^{III} to Eu^{III} occurs quickly. In $[Eu_x,Tb_{1-x}]$(**L**)-htpa, the Tb**L** emissions gradually shift to Eu**L** emissions with an increase in the Eu content. The luminescence lifetime of Tb^{III} in Tb**L**-htpa at 77 K is 0.49 ms, in which a new decay component of 0.02 ms is added with the mixing of Eu**L** in Tb**L**-htpa. The luminescence lifetime of Eu^{III} does not change under any mixing conditions of Eu^{III} and Tb^{III}. These luminescence observations of $[Eu_x,Tb_{1-x}]$(**L**)-htpa result from the effective energy transfer from Tb^{III} to Eu^{III} in the new network structure. The rate constant of MMEnT (k_{MMEnT}) can be qualitatively discussed, in which the k_{MMEnT} of $[Eu_x,Tb_{1-x}]$(**L**)-atpa will become much larger than that of $[Eu_x,Tb_{1-x}]$(**L**)-htpa.

It is remarkable that the MMEnT is observed in $[Eu_x,Tb_{1-x}]$(**L**)-atpa and $[Eu_x,Tb_{1-x}]$(**L**)-htpa but not in $[Eu_x,Tb_{1-x}]$(**L**)-bdc. This result indicates that the electronic structure of Ln**L** is maintained in a chain arrangement with bdc as a linker, leading to dual emissions from Eu^{III} and Tb^{III}. In contrast, in an amorphous network structure with atpa and htpa, the Ln**L**s are orientated at sufficient distance for an efficient MMEnT (Figure 6).

CONCLUSION

A series of novel chain-structured mixed Ln complexes with ff emissions, $[Eu_x,Tb_{1-x}]$(**L**)-bdc, $[Eu_x,Tb_{1-x}]$(**L**)-atpa and $[Eu_x,Tb_{1-x}]$(**L**)-htpa, were prepared and characterized. The structures of these chain complexes were clarified by synchrotron XRPD observations. The interchain distance of Ln**L**-bdc was estimated to be 14.36 Å. In the chain structure, the Ln ions exist at intervals of 12.29 Å along an *a* axis. These chain structures show thermal stability, thus retaining their photophysical properties even after heat treatment at ~200 °C. Depending on the linker and chain network structure, the chain-structured lanthanide complexes show dual emissions from each metal ion and/or sensitized emissions through MMEnT.

ACKNOWLEDGEMENTS

Synchrotron radiation experiments were performed at the BL02B2 of SPring-8 with the approval of the Japan Synchrotron Radiation Research Institute (JASRI; Proposal No. 2013B1776, 2013A1020 and 2011B1893). This work was partly supported by the Grants-in-Aid of MEXT for Scientific Research on Innovative Areas of 'Fusion Materials: Creative Development of Materials and Exploration of Their Function through Molecular Control (Area Number: 2206)' (No. 23107528 and 25107730), Challenging Exploratory Research (No. 23656544) Young Scientists A (No. 20685011), Young Scientists B (No. 70406833) and the Supported Program for the Strategic Research Foundation at Private Universities, 2013–2017, with a matching fund subsidy.

1 Masoomi, M. Y., Morsali, A. Applications of metal-organic coordination polymers as precursors for preparation of nano-materials. *Coord. Chem. Rev.* **256**, 2921–2943 (2012).
2 Higuchi, M. Electrochromic organic–metallic hybrid polymers: fundamentals and device applications. *Polym. J.* **41**, 511–520 (2009).
3 Doherty, C. M., Buso, D., Hill, A. J., Furukawa, S., Kitagawa, S., Falcaro, P. Using functional nano- and microparticles for the preparation of metal-organic framework composites with novel properties. *Acc. Chem. Res.* **47**, 396–405 (2014).
4 Bradshaw, D., Garai, A., Huo, J. Metal-organic framework growth at functional interfaces: thin films and composites for diverse applications. *Chem. Soc. Rev.* **41**, 2344–2381 (2012).
5 Betard, A., Fischer, R. A. Metal-organic framework thin films: from fundamentals to applications. *Chem. Rev.* **112**, 1055–1083 (2012).
6 Hosseini, M. W. Molecular tectonics from simple tectons to complex molecular networks. *Acc. Chem. Res.* **38**, 313–323 (2005).

7 He, H., Ma, H., Sun, D., Zhang, L., Wang, R., Sun, D. Porous Lanthanide-organic frameworks: control over interpenetration, gas adsorption, and catalyst properties. *Cryst. Growth Des.* **13**, 3154–3161 (2013).
8 Lan, Y. Q., Jiang, H. L., Li, S. L., Xu, Q. Mesoporous metal-organic frameworks with size-tunable cages: selective CO_2 uptake, encapsulation of Ln^{3+} cations for luminescence, and column-chromatographic dye separation. *Adv. Mater.* **23**, 5015–5020 (2011).
9 Natur, F. L., Calvez, G., Daiguebonne, C., Guillou, O., Bernot, K., Ledoux, J., Pollès, L. L., Roiland, C. Coordination polymers based on heterohexanuclear rare earth complexes: toward independent luminescence brightness and color tuning. *Inorg. Chem.* **52**, 6720–6730 (2013).
10 Li, Z., Zhu, G., Guo, X., Zhao, X., Jin, Z., Qiu, S. Synthesis, structure, and luminescent and magnetic properties of novel lanthanide metal-organic frameworks with zeolite-like topology. *Inorg. Chem.* **46**, 5174–5178 (2007).
11 D'Vries, R. F., Iglesias, M., Snejko, N., Alvarez-Garcia, S., Gutiérrez-Pueblaa, E., Monge, M. A. Mixed lanthanide succinate-sulfate 3D MOFs: catalysts in nitroaromatic reduction reactions and emitting materials. *J. Mater. Chem.* **22**, 1191–1198 (2012).
12 Decabt, R., Hecke, K. V., Depla, D., Leus, K., Weinberger, D., Driessche, I. V., Voort, P. V. D., Deun, R. V. Synthesis, crystal structures, and luminescence properties of carboxylate based rare-earth coordination polymers. *Inorg. Chem.* **51**, 11623–11634 (2012).
13 Lu, W. G., Jiang, L., Feng, X. L., Lu, T. B. Three-dimensional lanthanide anionic metal-organic frameworks with tunable luminescent properties induced by cation exchange. *Inorg. Chem.* **48**, 6997–6999 (2009).
14 Yu, Y., Ma, J. P., Dong, Y. B. Luminescent humidity sensors based on porous Ln^{3+}-MOFs. *Cryst. Eng. Commun.* **14**, 7175–7160 (2012).
15 Parker, D., Walton, J. W., Lamarque, L., Zwier, J. M. Comparative study of the luminescence properties and relative stability of a series of europium(III) complexes bearing one to four coordinated azaxanthone groups. *Eur. J. Inorg. Chem.* **25**, 3961–3966 (2010).
16 Soulie, M., Latzko, F., Bourrier, E., Placide, V., Butler, S. J., Pal, R., Walton, J. W., Baldeck, P. L., Le Guennic, B., Andraud, C., Zwier, J. M., Lamarque, L., Parker, D., Maury, O. Comparative analysis of conjugated alkynyl chromophore-triazacyclononane ligands for sensitized emission of europium and terbium. *Chem. Eur. J.* **20**, 8636–8646 (2014).
17 Amghouz, Z., Granda, S. G., García, J. R. Series of metal organic frameworks assembled from Ln(III), Na(I), and chiral flexible-achiral rigid dicarboxylates exhibiting tunable UV – vis – IR light emission. *Inorg. Chem.* **51**, 1703–1716 (2012).
18 Thielemann, D. T., Klinger, M., Wolf, T. J. A., Lan, Y., Wernsdorfer, W., Busse, M., Roesky, P. W., Unterreiner, A. N., Pawell, A. K., Junk, P. C., Deacon, G. B. Novel lanthanide-based polymeric chains and corresponding ultrafast dynamics in solution. *Inorg. Chem.* **50**, 11990–12000 (2011).
19 Cui, Y., Xu, H., Yue, Y., Guo, Z., Yu, J., Chen, Z., Gao, J., Yang, Y., Qian, G., Chen, B. A luminescent mixed-lanthanide metal – organic framework thermometer. *J. Am Chem. Soc.* **134**, 3979–3982 (2012).
20 Miyata, K., Konno, Y., Nakanishi, T., Kobayashi, A., Kato, M., Fushimi, K., Hasegawa, Y. Chameleon luminophore for sensing temperatures: control of metalto-metal and energy back transfer in lanthanide coordination polymers. *Angew. Chem.* **125**, 6541–6544 (2013).
21 Cadiau, A., Brites, C. D. S., Costa, P. M. F. J., Ferreira, R. A. S., Rocha, j., Carlos, L. D. Ratiometric nanothermometer based on an emissive Ln^{3+}-organic framework. *ACS Nano* **7**, 7213–7218 (2013).
22 D'vries R. F., Álvarez-García S., Snegko N., Bausá L. E., Puebla E. G., de Andrés A., Monge M. A. Multimetal rare earth MOFs for lighting and thermometry: tailoring color and optimal temperature range through enhanced disulfobenzoic triplet phosphorescence. *J. Mater. Chem. C* 2013; **1**: 6316–6324.
23 Rao, X., Song, T., Gao, J., Cui, Y., Yang, Y., Wu, C., Chen, B., Qian, G. A Highly sensitive mixed lanthanide metal-organic framework self-calibrated luminescent thermometer. *J. Am. Chem. Soc.* **135**, 15559–15564 (2013).
24 Cui, Y., Zou, W., Song, R., Yu, J., Zhang, Q., Yang, Y., Qian, G. A ratiometric and colorimetric luminescent thermometer over a wide temperature range based on a lanthanide coordination polymer. *Chem. Commun.* **50**, 719–721 (2014).
25 Kobayashi, A., Suzuki, Y., Ohba, T., Noro, S., Chang, H., Kato, M. Ln-Co-based rock-salt-type porous coordination polymers: vapor response controlled by changing the lanthanide ion. *Inorg. Chem.* **50**, 2061–2063 (2011).
26 Hasegawa, M., Ohtsu, H., Kodama, D., Kasai, T., Sakurai, S., Ishii, A., Suzuki, K. Luminescence behaviour in acetonitrile and in the solid state of a series of lanthanide complexes with a single helical ligand. *New J. Chem.* **38**, 1225–1234 (2014).
27 Ohashi, H., Tanigaki, K., Kumashiro, R., Sugihara, S., Hiroshiba, S., Kimura, S., Kato, K., Takata, M. Low-glancing-angle x-ray diffraction study on the relationship between crystallinity and properties of C60 field effect transistor. *Appl. Phys. Lett.* **84**, 520–522 (2004).
28 Ishii, A., Habu, K., Kishi, S., Ohtsu, H., Komatsu, T., Osaka, K., Kato, K., Kimura, S., Takata, M., Hasegawa, M., Shigesato, Y. Novel emission properties of melem caused by the heavy metal effect of lanthanides(III) in a LB film. *Photochem. Photobiol. Sci.* **6**, 804–809 (2007).
29 Kawamura, Y., Sasabe, H., Adachi, C. Simple accurate system for measuring absolute photoluminescence quantum efficiency in organic solid-state thin films. *Jpn J. Appl. Phys.* **43**, 7729–7730 (2004).
30 Suzuki, K., Kobayashi, A., Kaneko, S., Takehira, K., Yoshihara, T., Ishida, H., Shiina, Y., Oishi, S., Tobita, S. Reevaluation of absolute luminescence quantum yields of standard solutions using a spectrometer with an integrating sphere and a back-thinned CCD detector. *Phys. Chem. Chem. Phys.* **11**, 9850–9860 (2009).
31 Kobayashi, A., Suzuki, K., Yoshihara, T., Tobita, S. Absolute measurements of photoluminescence quantum yields of 1-halonaphthalenes in 77 K rigid solution using an integrating sphere instrument. *Chem. Lett.* **39**, 282–283 (2010).
32 Wierzbicka, E., Boczar, M., Wójcik, M. J. Investigation of hydrogen bonds properties in the terephthalic acid. *Spectrochim. Acta A* **130**, 488–493 (2014).

Supplementary Information accompanies the paper on Polymer Journal website (http://www.nature.com/pj)